Environ Geol (2005) 47: 535–546
DOI 10.1007/s00254-004-1176-z

ORIGINAL ARTICLE

Wen–Cheng Liu

Modeling the influence of settling velocity on cohesive sediment transport in Tanshui River estuary

Received: 14 June 2004
Accepted: 13 September 2004
Published online: 8 December 2004

W. Liu
Department of Civil and Disaster Prevention Engineering,
National United University,
Miao–Li 360, Taiwan
Tel.: +886-37-381674
Fax: +886-37-326567

Abstract Settling velocities of suspended cohesive sediment in estuaries vary over a range of several orders in magnitude. Variations in the suspended sediment concentration are often considered as the principal cause. Turbulence and the suspended sediment concentration, as well as other factors such as salinity, dissolved organic substances, flocculation ability, and the rate of floc growth affect setting velocities. A laterally–averaged finite difference model for hydrodynamics and cohesive sediment transport is developed and applied in the Tanshui River estuary, Taiwan. The model has been calibrated and verified with water surface elevation, longitudinal velocity, salinity, and cohesive sediment measured. The overall performance of the model is in qualitative agreement with the available data. The model is used to investigate the influence of settling velocity on cohesive sediment transport dynamics. The simulation indicates that the turbidity maximum zone is near Kuan–Du. When settling velocities increase the surface cohesive sediment concentration at Kuan–Du station trends to decrease and bottom cohesive sediment concentration increases. Both surface and bottom cohesive sediment concentrations decrease at Taipei Bridge and Pa–Ling Bridge. This implies that suspended sediment advected seaward and deposited. There is consequently a net seaward flux of suspended sediment near surface, and a net landward flux near the bed.

Keywords Cohesive sediment transport · Settling velocity · Salinity · Turbidity maximum · Tanshui River estuary · Taiwan

Introduction

The filtering role of estuaries makes them crucial transitional areas trapping significant quantities of particulate and dissolved matter through a wide variety of physical and biogeochemical processes. Cohesive sediments play an important role in these processes. Fine, cohesive sediments in estuaries are comprised largely of clay–sized particles. The remainder may include fine silts, biogenic detritus, organic matter, waste materials, and sometimes small quantities of very fine sand. The electrical surface forces of attraction and repulsion, which act on each elementary clay particle, are several orders of magnitude larger than gravitational force. As a result, the physico–chemical properties of fine sediments are controlled mostly by surface forces.

In water with a very low salinity (less than about one part per thousand, ppt) the elementary particles are usually found in a dispersed state. A slight increase in the salinity up to 2–3 ppt is sufficient to enable the particles to coagulate to form units known as flocs (Krone 1978). Each floc may consist of thousands of

elementary particles. Coagulation of elementary particles depends upon inter–particle collision and cohesion resulting from collision. The three principle mechanisms of inter–particle collision in suspension are Brownian motion, internal fluid shearing and differential sedimentation (Einstein and Krone 1962). Cohesion of particles is caused by the presence of net attractive inter–particle surfaces. The latter condition is caused by the increased concentration of dissolved ions, which serves to depress the charged ionic double layer around each particle and allow the attractive forces to predominate over the double dependent repulsive forces (Olphen 1963).

In an estuarine environment, many factors including erosion, advection, dispersion, aggregation, settling, deposition, and consolidation of the deposit may affect the transport processes of cohesive sediment. Under low flow velocities, sometimes coupled with turbulent conditions which favor the formation of large aggregates, fine sediments have a tendency to deposit in dredged cuts and navigation channels, in harbors and marines, and behind pilings in water (Krone 1978). In addition, the mixing zone between upland fresh water and seawater in estuaries is a favorable site for bottom sediment accumulation. In as much as estuaries are often used as transport routes, it is essential to be able to accurately estimate the amount of dredging required to maintain navigable depths in these water bodies.

Hydrodynamic action is the most important mechanism involved in sediment transport (Kuo and others 1978). It advects the suspended sediments, provides the force needed to erode the bed and, through turbulence, plays a major role in the flocculation of cohesive sediments. Relatively large velocities generally occur in tidal estuaries. Because the hydrodynamic processes involved in sediment transport are mainly non–linear, the sediments are very mobile in these estuaries. They are eroded during slack water, eroded again and transported downwards during ebb and redeposited during the next slack water, to restart their movement in the forthcoming tidal cycle.

Settling velocities of suspended fine–grained sediment in estuaries vary over a range of several orders in magnitude. Variations in the suspended sediment concentration are often put forward as the principal cause (Wollast 1986). In this study, a vertical two–dimensional finite difference barotropic and baroclinic model for hydrodynamic and cohesive sediment transport is presented to investigate the influence of settling velocity on cohesive sediment transport under low flow conditions in the Tanshui River estuary.

The Tanshui estuary, located on the Taipei, is the largest tidal river in Taiwan. The river system has a total drainage area of 2,726 km^2, a total channel length of 327.6 km, and consists of three major tributaries: (1) The Tahan Stream; (2) Hsintien Stream; and (3) Keelung River (Fig. 1). The Tahan Stream and Hsintien Stream join at Wan–Hwa, Taipei City; afterward, the estuarine system combines with the Keelung River in Kuan–Du, Taipei country. The segment of the estuary from Wan–Hwa to the estuarine mouth is called the Tanshui River. The downstream reaches of all three tributaries are influenced by tide. The upriver reaches are affected by daily varying freshwater discharge. Semi–diurnal tides are the principal tidal constituents, with a mean tidal range of 2.22 m and a spring tidal range of 3.1 m. The average river discharges are 62.1 m^3/s, 72.7 m^3/s, 26.1 m^3/s, respectively, in the Tahan Stream, Hsintien Stream and Keelung River. The mean annual river discharge and suspended par-

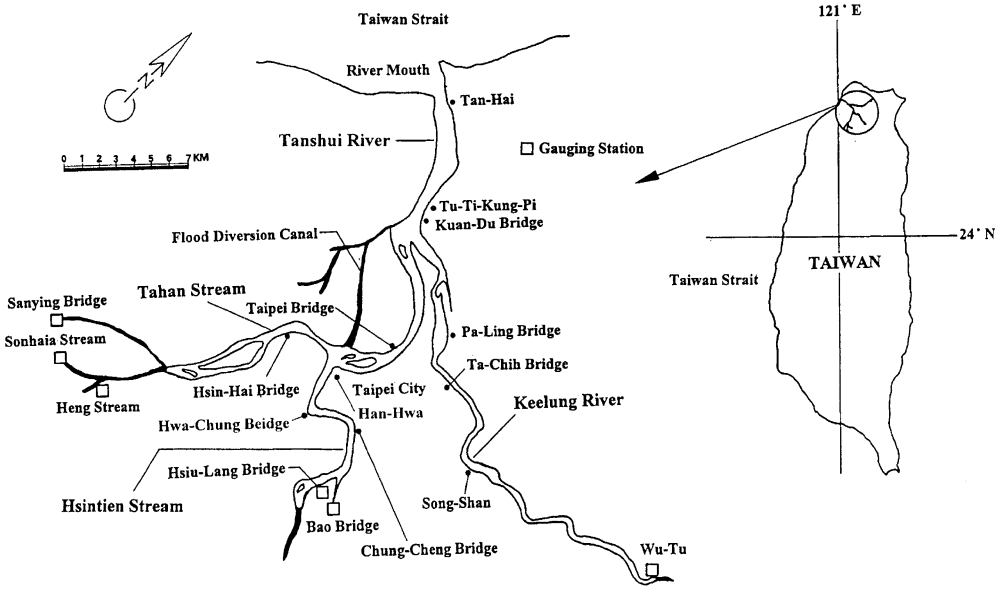

Fig. 1 The map of the Tanshui River estuarine system

ticulate matter transport over the last 40 years have been approximately 7,044x10^6 m^3/y and 11.45x10^6 t/y, respectively (Water Resources Agency 1999). In addition to the barotropic flows forced by tide and river discharge, the baroclinic flow forced by seawater intrusion is another important transport mechanism in the Tanshui River estuary system.

Materials and methods

Hydrodynamic model

The laterally integrated two–dimensional hydrodynamic model developed by Kuo and others (1978) was modified for application to the Tanshui River estuarine system. The original version is applicable only to a single stem estuary. The model is expanded to include the simulation of tributaries that is necessary because of the three major tributaries in the tidal portion of the system. Assumptions for the validity of the governing equations are: (1) variations of dependent variables in the transverse direction are small and negligible and (2) the lateral average of the transverse velocity component is zero. The hydrostatic approximation and the Boussinesq approximation are also assumed to be valid (Blumberg 1977). With a right–handed Cartesian coordinate system with the x–axis directed seaward and the z–axis directed upward (Fig. 2), the governing equations should be written as followings.

The continuity equations are

$$\frac{\partial(uB)}{\partial x}+\frac{\partial(wB)}{\partial z}=q_p \tag{1}$$

where u and w = laterally averaged velocities in the x– and z– directions, respectively, B = river width, q_p = lateral inflow per unit bank area, and

$$\frac{\partial}{\partial t}(B_\eta\eta)+\frac{\partial}{\partial x}\int_{-H}^{\eta}(uB)dz=q \tag{2}$$

where t = time, η = position of the free surface above mean sea level, $B\eta$ = river width at the free surface including side storage area, H = total depth below mean sea level, q = lateral inflow per unit river length. Eqs. (1) and (2) are the laterally and sectionally, respectively, integrated continuity equations for incompressible flow.

The momentum balance equation is

$$\frac{\partial(uB)}{\partial t}+\frac{\partial(uBu)}{\partial x}+\frac{\partial(uBw)}{\partial z}=-\frac{B}{\rho}\frac{\partial p}{\partial x}+\frac{\partial}{\partial x}\left(A_xB\frac{\partial u}{\partial x}\right)+\frac{\partial}{\partial z}\left(A_zB\frac{\partial u}{\partial z}\right) \tag{3}$$

where p and ρ = pressure and density, respectively, A_x and A_z = turbulent viscosities in the x– and z– directions, respectively. This is the laterally integrated equation of motion for incompressible, but non–homogeneous flow and represents the momentum balance along the longitudinal axis of an estuary.

The hydrostatic equation is

$$\frac{\partial p}{\partial z}=-\rho g \tag{4}$$

where g = gravitational acceleration. When the hydrostatic approximation (i.e., gravity is the dominant force in the vertical direction) is applied to the equation of motion in the z– direction, the result is the hydrostatic solution given by Eq. (4).

The laterally integrated mass balance equation for dissolved salt is

$$\frac{\partial(sB)}{\partial t}+\frac{\partial(sBu)}{\partial x}+\frac{\partial(sBw)}{\partial z}=\frac{\partial}{\partial x}(K_xB\frac{\partial s}{\partial x})+\frac{\partial}{\partial z}(K_zB\frac{\partial s}{\partial z})+S_o \tag{5}$$

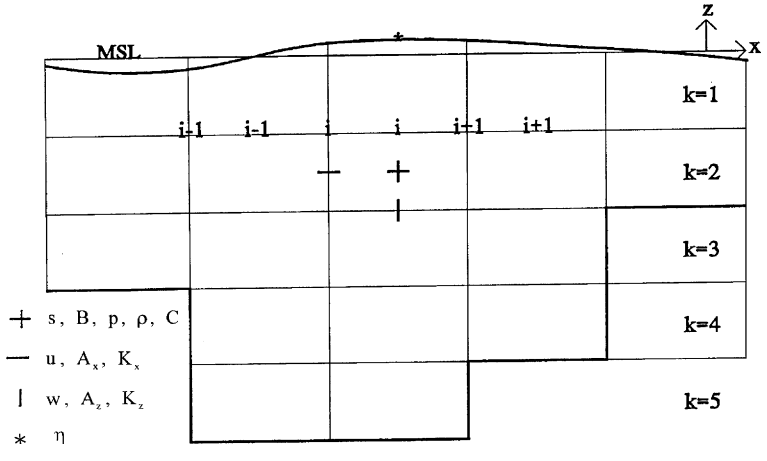

Fig. 2 Grid pattern, location and indexing of variables

where s = laterally averaged salinity, K_x and K_z = turbulent diffusivities in the x− and z− directions, respectively, S_o = source and sink of salt water.

The equation of state is

$$\rho = \rho_o(1 + ks) \tag{6}$$

where ρ_o = density of fresh water and a constant $k = 7.5\text{x}10^{-4}$ ppt^{-1}. The density is related to the salinity by the simplified equation of state [Eq. (6)], which is usually regarded as a satisfactory approximation because of the large spatial gradients of salinity in estuaries (Hamilton 1977).

The turbulent closure model uses the Munk−Anderson type formulations:

$$A_{z=}\alpha Z^2\left(1-\frac{Z}{h}\right)^2\left|\frac{\partial u}{\partial z}\right|(1+\beta R_i)^{\frac{-1}{2}} \tag{7}$$

$$K_{z=}\alpha Z^2\left(1-\frac{Z}{h}\right)^2\left|\frac{\partial u}{\partial z}\right|(1+\beta R_i)^{\frac{-3}{2}} \tag{8}$$

where Z and h = distance from the surface and total depth ($h = \eta + H$) ,R_i = local Richard number, α, β = constants. The system of equations is solved using finite difference method with uniform grid of spatially staggered variables. Eqs. (1) and (3) are solved to obtain the time−varying solution of the free surface (η) and laterally averaged velocity fields (u and w). The pressure term (p) is evaluated using Eq. (4) with the water density (ρ) from Eq. (6), and salinity (s) using Eq. (5). The detailed description of the method of solution including boundary conditions, turbulence closure model, treatment of the interaction of tributaries and main stem, and stability criteria can be found in Hsu and others (1996, 1997).

The present model has two options for the turbulence closure model: (a) Eqs. (7) and (8); and (b) the Mellor and Yamada Level 2 turbulence model (Mellor and Yamada 1982). The second option was not adopted when the model was applied to the Tanshui River estuarine system because it produced overly stratified salinity distribution compared to the field observation. When the Richardson number is higher than the critical value (about 0.2), the Mellor and Yamada Level 2 model turns off the vertical mixing completely, which results in over−stratification in the model results (Hsu and others 1996, 1997).

The layout of the grid system used in the model and locations of variables within the grid are shown in Fig. 2. The grid system has η defined at the middle of each segment, while s, B, ρ and p are at the center of the grid cell. The variables, w, A_z and K_z, are defined at the bottom face of the grid cell, while the grid containing u, A_x and K_x is staggered by half the segment length as these are defined at the grid cell walls. The staggered grid structure, also used by many other investigators, permits easy application of the boundary conditions and evaluation of the dominant pressure gradient force without interpolation or averaging (Blumberg 1977).

Sediment transport model

The sediment transport is based on the equation describing the mass−balance where the vertical advection includes the particle settling velocity. The equations that are solved by the finite difference method have the form:

$$\frac{\partial(CB)}{\partial t}+\frac{\partial(CBu)}{\partial x}+\frac{\partial(CB(w-W_s))}{\partial z} = \frac{\partial}{\partial x}\left(K_xB\frac{\partial C}{\partial x}\right)+\frac{\partial}{\partial z}\left(K_zB\frac{\partial C}{\partial z}\right)-Bd+Br+q_pC_t \tag{9}$$

where C = suspended sediment concentration, W_s = sediment fall velocity, d = sediment deposition rate, r = sediment suspension rate, C_t = sediment concentration of lateral inflow.

The physical parameters (u, w, K_x, and K_z) in the physical transport in Eq. (9) are provided from the hydrodynamic model. The physical transport terms, both advective and identical for suspended sediment, are treated in the same manner as those in the mass balance equation for salt [Eq. (5)]. The last two terms of Eq. (9) represent the sink and source due to the deposition and erosion of the suspended sediment.

Settling velocity

The vertical transport is due to vertical advection, particle settling or turbulent diffusion. The hydrodynamic model computes the vertical velocity and the turbulent diffusive. The settling velocity depends on the gravitational forces, and on the vertical shear due to settling movement. The gravitational forces depend on the density of each individual particle forming flocs and on the floc porosity occupied by water.

The frictional forces depend on the form of the floc and on the Reynolds number of the surrounding flow during settling. For very small bodies, the flow is laminar and the ratio between the gravitational and the frictional force is proportional to the reciprocal of the diameter of the floc. Therefore, the settling velocity is expected to increase with floc size. Unfortunately, large flocs can have smaller density and there is no unique relation between floc size and settling velocity.

Probability of particles to aggregate into flocs depends on the probability of the particles to collide. The probability is proportional to the concentration, and also increases with the amplitude and frequency of the

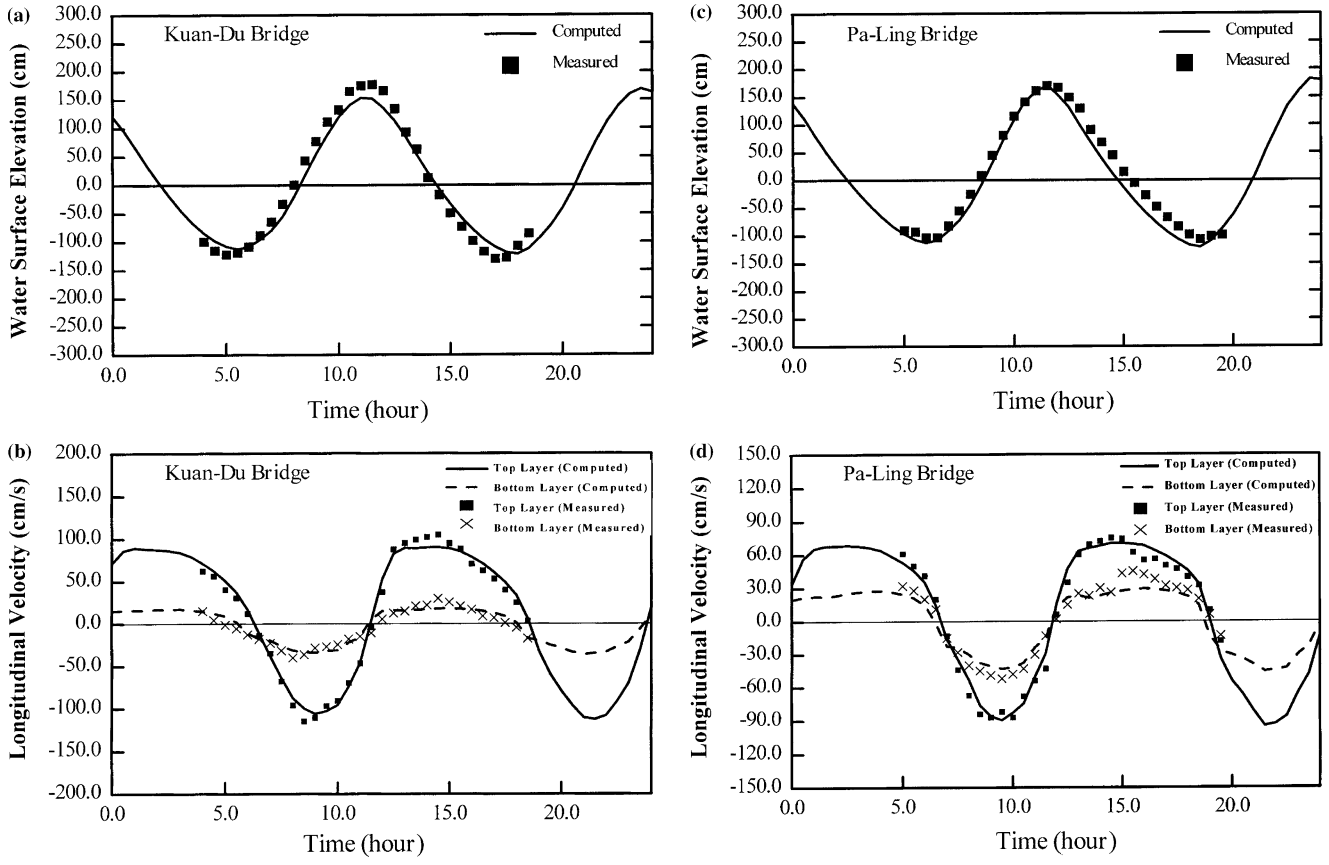

Fig. 3a–d Examples of model verification results: Comparison of measured and computed results on April 16, 1999 (**a**) water surface elevation (Kuan–Du Bridge); (**b**) longitudinal velocity (Kuan–Du Bridge); (**c**) water surface elevation (Pa–Ling Bridge); (**d**) longitudinal velocity (Pa–Ling Bridge)

turbulent random movement. Aggregation is a reversible process. Flocs are fragile and, if submitted to shear, they can disaggregate, because shear increases also with turbulent intensity; the latter plays a double role in the aggregation process.

The concentration and the turbulent intensity determine the probability of the two particles to meet. To form a floc, the particles must collide but, in addition, they must adhere to each other. Gluing forces depend on the type of particles, and also on the ionization of the environment. The latter is a function of the salinity, however, there is no correlation relating salinity and flocculation. From field work (Wollast 1986), there is clear evidence that an intensive flocculation occurs as soon as salinity reaches about 1 ppt and is complete for values higher than 2.5 ppt.

The model representing cohesive sediment by a bulk concentration uses a bulk settling velocity. If no information is available on the type of particles in the system and no evolution equation is solved for each class of flocs, then it is not possible to explicitly represent the flocculation processes in this type of correlation. The general correlation for the settling velocity is:

$$W_s = KC^m \tag{10}$$

The coefficient K (m^4/kg s) depends on the mineralogy of the mud and the exponents m depend on particle size and shape.

Results and discussion

Model calibration and verification

In the application to the Tanshui estuarine system, the model treats the Tanshui River and Tahan Stream as the main stem and Hsintien Stream and Keelung River as tributaries. They are divided into 33, 14, and 37 segments, respectively, with a uniform segment length of 1.0 km. Because surface elevation at low tide is about 1.5 m below mean sea level at spring tide, the thickness of the top layer is 2.0 m to maintain the surface elevation above the bottom of the layer at all times. The thickness of other layers is 1.0 m. The measured cross–sectional profiles in each segment were averaged and schematized. First, the bottom elevation was determined at an integral number of meters below the

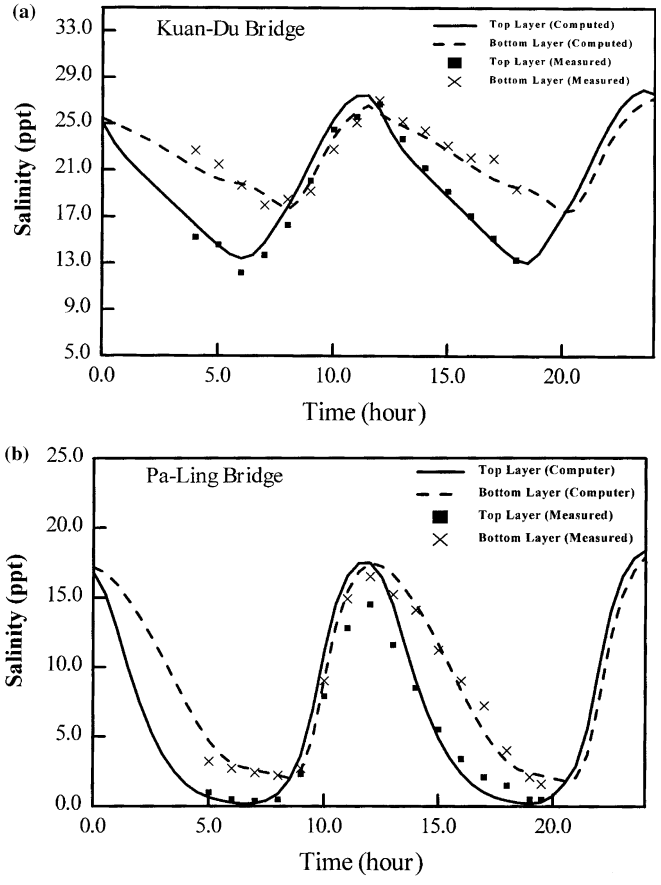

Fig. 4a, b Comparison of computed salinity with time series data on April 16, 1999 (**a**) Kuan–Du Bridge; (**b**) Pa–Ling Bridge

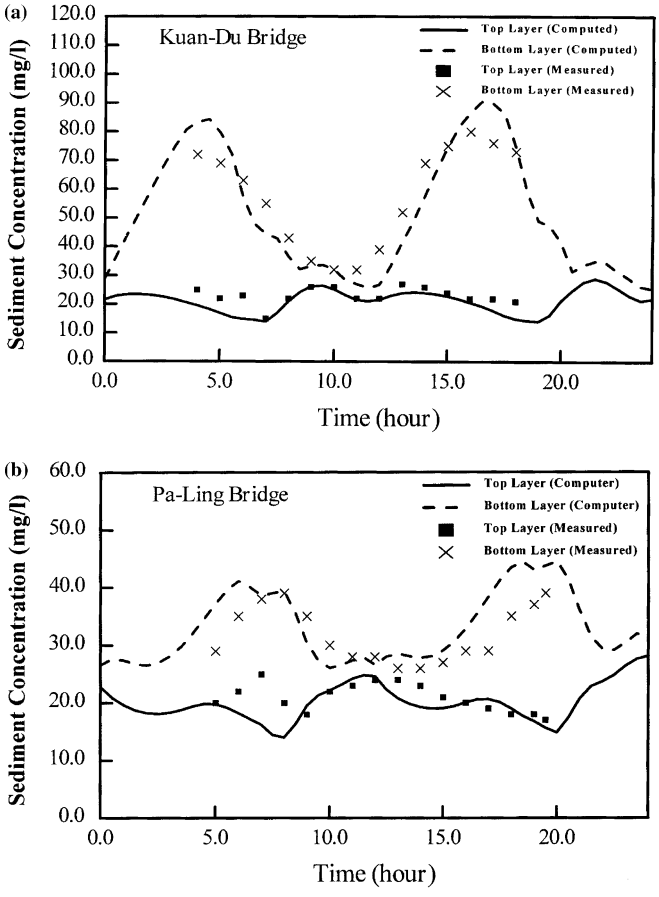

Fig. 5a, b Comparison of computed and field measured cohesive sediment concentration on April 16, 1999 (**a**) Kuan–Du Bridge; (**b**) Pa–Ling Bridge

mean sea level. Then the width at each layer was determined while maintaining the cross–sectional area roughly to be the same as in the measured profiles. To seek reasonable boundary conditions that are not influenced by the tidal, the computational domain is extended beyond the tidal limits in the main stem and in the tributaries. Time–varying boundary conditions consisting of freshwater inflows through the upstream boundaries of the three branches, and the tide and salinity at the river mouth were specified for the model run. The upstream boundary conditions were daily freshwater discharges at Cheng–Ling Bridge (Tahan Stream), Hsui–Lang Bridge (Hsintien Stream), and Wu–Tu station (Keelung River). Hourly tidal elevations measured at the river mouth were used as one of the downstream boundary conditions. The maximum salinity measured at the mouth on survey data were linearly interpolated in time and used for the boundary condition, which specified the high tide salinity at each tidal cycle.

Manning's friction coefficient and the two free parameters in the expression for the turbulent diffusion coefficients are primary parameters requiring calibration

Table 1 The amplitudes and phases of the primary 9 tidal constituents at the Tanshui River mouth

Constituents	Amplitude (cm)	Phase (degree)
M2	104.87	35.60
S2	27.85	−7.18
N2	21.33	−43.76
K1	19.94	−133.79
Sa	17.06	−143.32
O1	16.22	−47.96
K2	7.17	131.50
P1	7.14	−110.58
M4	2.83	47.44

in the hydrodynamics model. For the calibration and verification of the model with respect to surface elevation, longitudinal velocity and salinity was conducted covering the period during which field measurements were taken in 1996 and 1999. The data consist of two 13–hour time series at four stations. Measurements were made at 30–minute intervals over a full tidal cycle by Taiwan Water Resources Agency on April 18, 1996 and

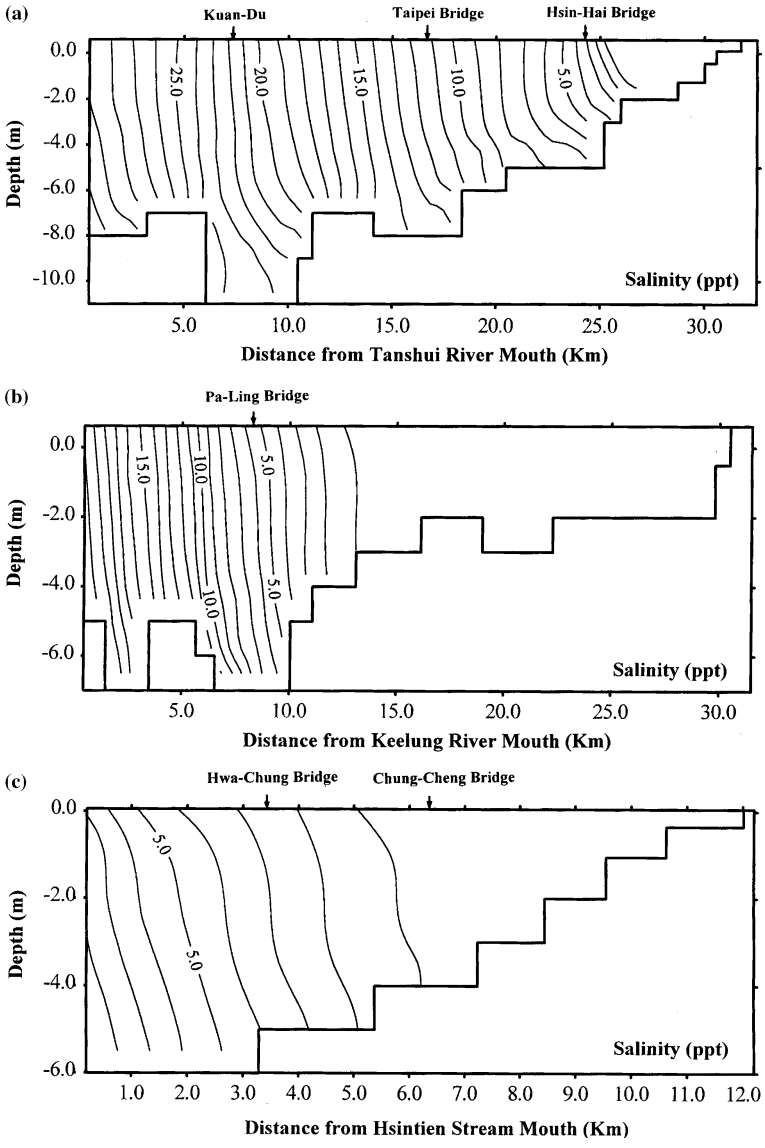

Fig. 6a–c Calculated salinity distributions averaged over 58 tidal cycles (**a**) Tanshui River–Tahan Stream; (**b**) Keelung River; (**c**) Hsintien Stream

April 16, 1999. The values of Manning's friction coefficient were adjusted until a best fit was obtained between computed and observed surface elevation and current velocity on April 18, 1996. Then the model was run to simulate the condition on April 16, 1999 without further adjustment of Manning's friction coefficient. Figure 3 presents examples of the comparisons between model results and field observations for model verification. The overall agreement between the model results and field data are satisfactory. The calibrated and verified model has the Manning's friction coefficient ranging from 0.032 to 0.036 in Tanshui River–Tahan Stream, 0.015 for the Hsintien Stream, and from 0.023 to 0.016 for the Keelung River. The constants in the turbulence model were determined through comparisons of salinity distribution between those computed and observed (shown in Fig. 4). The calibrated and verified constants for the turbulence model are $\alpha = 0.0115$ and $\beta = 0.75$ in Eqs. (7) and (8).

Measurements of suspended sediment concentrations in the Tanshui River estuary on April 18, 1996 and April 16, 1999 were used to calibrate and verify the cohesive sediment transport model. Data of suspended sediment at upstream boundaries and downstream boundary were obtained from Taiwan Environmental Protection Administration. The critical shear stress for deposition was set to 0.5 dyne/cm^2, and the critical shear stress for erosion assumed to be 1.0 dyne/cm^2. The settling velocity formula for flocculation is set $m = 1$ and $K = 5.0\text{x}10^{-3}$ m^4/kg s, using the model simulation. Figure 5 shows a comparison of field–measured data and model–predicted suspended cohesive sediment concentration variations with time for model verification on April 16, 1999. The results generally show reasonable

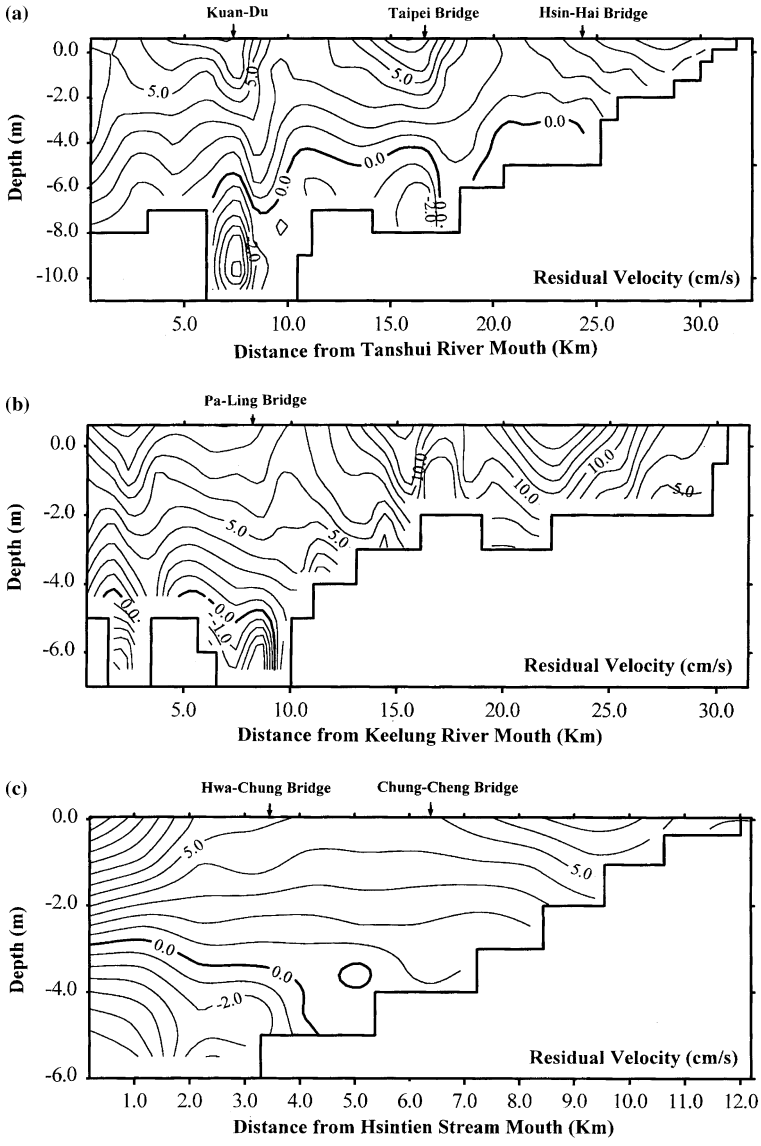

Fig. 7a–c Calculated residual current (**a**) Tanshui River–Tahan Stream; (**b**) Keelung River; (**c**) Hsintien Stream

agreement between the model predictions and field–measured data.

Model application

The validated model was used to perform model simulations in the Tanshui River system. The values of all coefficients of the numerical model have been determined by calibration and verification processes; no further adjustment to the coefficients was made. The time series data of surface elevation at river mouth, collected by the Taiwan Water Resources Agency, were examined and harmonic analyses were performed. Residual surface elevation and energy ratio are used to judge the harmonic results. Residual surface elevation is the Root–mean Square of the difference between the synthetic tide and observed surface elevation and the energy ratio represents the ratio of energy of water surface fluctuation of synthetic tide to that of observed tide. Hsu and others (1999) and Liu and others (2001) concluded that nine constituent tides represent adequately the tidal conditions. Therefore, a nine–constituent tide was used to specify the downstream boundary condition for the following model experiments. For the harmonic analysis, the surface elevation η is presented in the form:

$$\eta(t) = \langle\eta\rangle + \sum\nolimits_k a_k \cos(\sigma_k t - \phi_k) \tag{11}$$

where a_k and ϕ_k are the amplitude and phase angle of the kth harmonic, respectively; $\langle\eta\rangle$is the mean surface elevation; σ_k is angular velocity. Table 1 lists the amplitudes and phases of the primary nine tidal constituents at the river mouth. Historical long–term mean

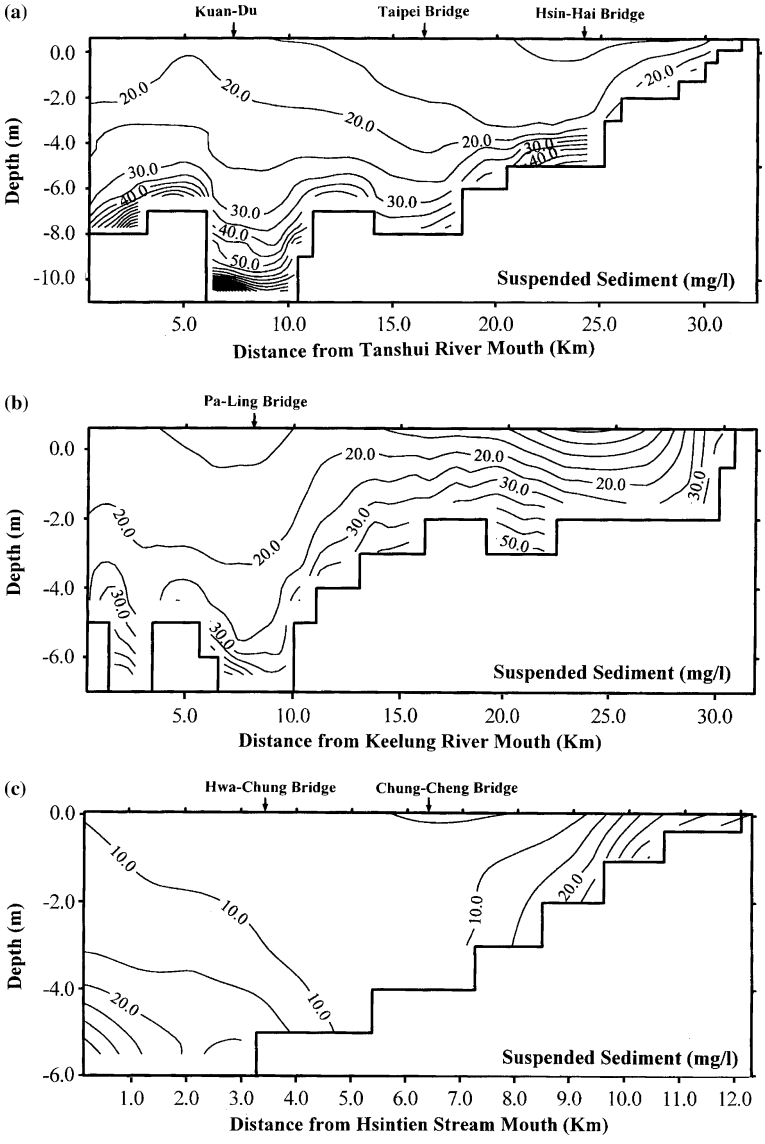

Fig. 8a–c Calculated suspended sediment concentration as $K = 5.0\times10^{-3}$ m^4/kg s (**a**) Tanshui River–Tahan Stream; (**b**) Keelung River; (**c**) Hsintien Stream

(15–year average) water surface elevation is +6.5 cm relative to mean sea level. For the first model simulation, historical long–term mean (34–year average) discharges were used for the upriver boundary conditions in the tributaries. Q_{90} freshwater discharges (the annually flow is equaled or exceeded 90% of time) at the tidal upstream limits of the three major tributaries are 4.0 m^3/s, 6.9 m^3/s and 1.3 m^3/s for the Tahan Stream, Hsintien Stream and Keelung River, respectively. Salinity at the Tanshui River mouth was set at 32 ppt under Q_{90} flow condition. In the sediment transport model, a concentration characteristic of the river mouth is 20 mg/l. The river boundary was in the limit of the tidal propagation of three tributaries, and a constant value was also imposed–40 mg/l. The model was run for an one–year duration (705 tidal cycles).

Different K values of the settling velocity formula in Eq. (10) are used to investigate the effect on cohesive sediment transport and the K values adopted are 1.0×10^{-3} m^4/kg s, 3.0×10^{-3} m^4/kg s, and 5.0×10^{-3} m^4/kg s representing different settling velocities in the sediment transport model. The calculated results of hydrodynamic in the Tanshui River estuarine system are presented in Figs. 6 and 7. Figure 6 presents the average salinity distribution over two spring–neap cycles (i.e., 58 tidal cycles) in the Tanshui River–Tahan Stream, Keelung River and Hsintien Stream. The limits of salt intrusion are at Hsin–Hai Bridge in the Tahan Stream, 13 km from the Keelung River mouth, and 6 km from the Hsintien Stream mouth. The average residual velocities over two spring–neap cycles are presented in Fig. 7, and indicate a general upriver residual flow along the bottom at the

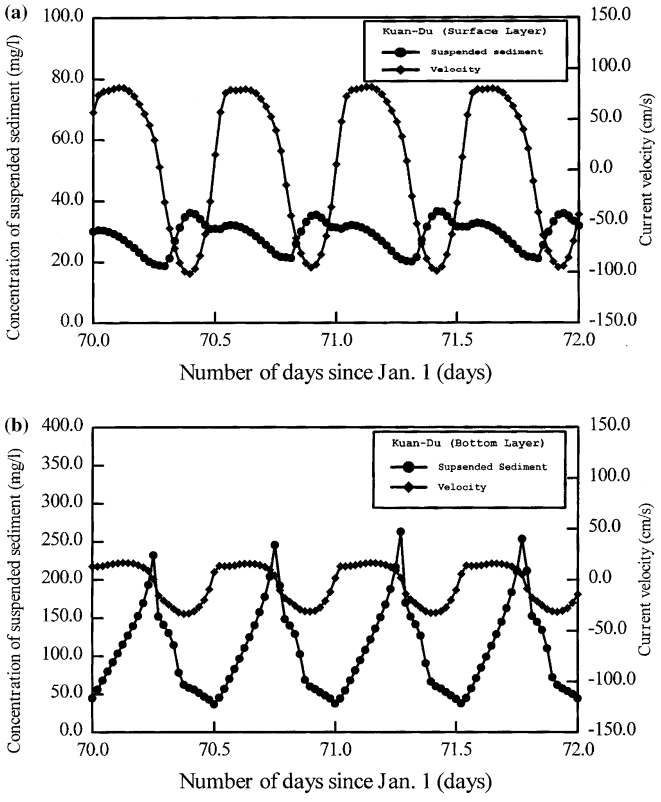

Fig. 9a,b Tidal cycle variation of current velocity and suspended sediment concentration at Kuan–Du station (**a**) surface layer; (**b**) bottom layer

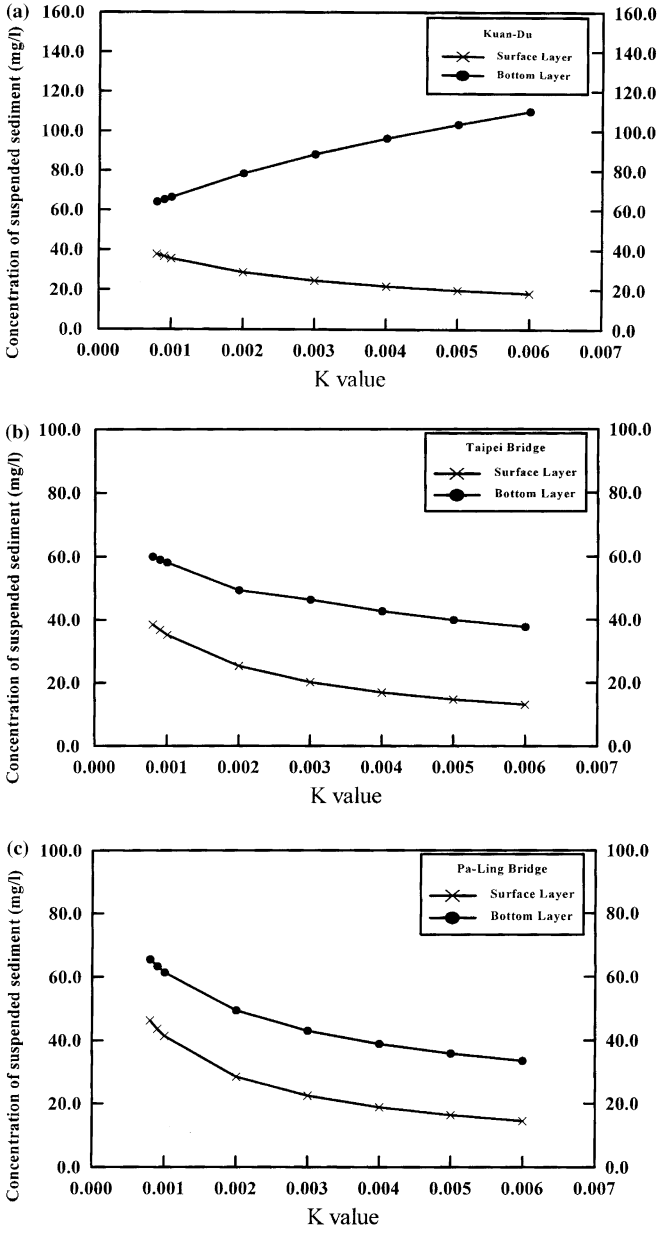

Fig. 10a–c Magnitude of the concentration as a function of particle settling velocity, K, at the surface and bottom layers (**a**) Kuan–Du; (**b**) Taipei Bridge; (**c**) Pa–Ling Bridge

lower portions of all three rivers. There exists a null point at the upriver limit of upriver bottom flow where bottom flows converge. The extensive intrusion of saline water introduces a significant baroclinic forcing and induces a strong residual circulatory system in the estuary. Contours of the suspended sediment distribution (Fig. 8) in the formulation of settling velocity as $m=1$ and $K=5.0\times10^{-3}$ m^4/kg s used show the presence of a concentration, or turbidity maximum approximately 7.5 km (Kuan–Du) from the river mouth. This corresponds closely to the maximum vertical velocity associated with the estuarine circulation.

Figure 9 shows the tidal cycle variation of longitudinal velocity and suspended sediment concentrations. As the tidal wave celerity is a function of water depth, the crest (at high water) propagates faster than the trough (at low water). This causes the ebb period to become longer and the flood duration shorter, resulting in an asymmetrical tidal curve. In addition, as nearly the same quantity of water should flow in either direction for each tide, this asymmetric tidal cycle induces higher flood velocities than ebb velocities. The deformation of the tidal wave also induces an asymmetry between slack durations: the high water slack is longer while the low water one is shorter (Postma 1967).

As the rate of erosion of cohesive sediment is a function of the bottom shear stress (Partheniades 1965), the higher flood tide velocities cause a greater bottom erosion and suspended sediment transport than the ebb. This leads to a net upstream movement of sediment near the bed, until the point of the estuary where the velocity due to the river flow is dominant for the transport. The current velocities show considerable diurnal variation, but the residual water flow is seaward near the surface and landward near the bed (Kuan–Du). There is con-

sequently a net seaward flux of suspended sediment near the surface, and a net landward flux near the bed. The maximum suspended sediment concentration occurs near the bottom and has hysteresis effects with maximum current (Fig. 9b)

Dependence of the magnitude of the maximum suspended sediment concentration on settling velocity (K value) is better exemplified in Fig. 10. When the settling velocities increase, the suspended sediment concentrations decrease at the surface and bottom layers of Taipei Bridge and Pa−Ling Bridge (Fig. 10b and c). The suspended sediment concentrations increase in the bottom layer of Kuan−Du, when the settling velocities increase (Fig. 10a). At the downriver stations, particularly at Kuan−Du where salinity is high and water depth is large, baroclinic forcing increases with freshwater discharge at low flow. The settling velocity seems to act mainly on the suspension pattern at Kuan−Du and, thus, on the availability of the bottom sediment. As a functional link exists between deposits and suspended sediment, the variation of this particle characteristic also acts on the turbidity maximum behavior. The asymmetric tidal wave propagation is characterized by a stronger flood (compared to the ebb currents) and a longer high water slack than low water slack. This induced a tidal pumping of particles upward, until there is a decrease of the tide amplitude in the upper estuary.

Conclusions

A numerical model has been developed to study the hydrodynamic characteristics and cohesive sediment transport in the Tanshui River estuarine system. The model is a laterally integrated, two−dimensional, real−time model. The model has been calibrated and verified with observed time series water level, current, salinity and cohesive sediment concentration. The most important aspect of estuarine circulation is the gravitational circulation. The tidally−averaged circulation in a coastal plain estuary is dominated by the upstream movement of heavier saline water in the lower layer and the downstream movement of fresh water in the upper layer. The circulation pattern is driven by the longitudinal gradient of salinity distribution.

The tidally−averaged cohesive sediment concentration distribution, averaged over two spring−neap tidal cycles, are presented; a local maximum concentration exists around the null point. The effect of the tidal asymmetric is to favor sedimentation at slack water; the slack asymmetry induces a greater settling of particles from the turbidity maximum during high water than during low water. The mechanisms induce a net upstream movement of suspended sediment, which acts in creating a tidal sediment trap downstream. The simulation results show that the turbidity maximum zone is near Kuan−Du. When settling velocities increase the surface suspended sediment concentration at Kuan−Du tends to decrease and bottom suspended sediment concentration increases. This implies that suspended sediment advected seaward and deposited. There is consequently a net seaward flux of suspended sediment near surface, and a net landward flux near the bed.

Acknowledgment This study is supported, in part, by National Science Council, Taiwan, under grant No. NSC 92–2211−E−002–037. The writer also thanks the Taiwan Water Resources Agency and Environmental Protection Administration for providing the prototype data.

References

Blumberg AF (1977) Numerical tidal model of Chesapeake Bay. J Hydraul Div ASCE 103:295–319

Einstein HA, Krone RB (1962) Experiments to determine modes of cohesive sediment transport in salt water. J Geophy Res 67:1451–1464

Hamilton P (1977) On the numerical formation of a time dependent multi−level model of an estuary, with particular reference to boundary conditions. In: Estuarine Processes, Vol. II Circulation, Sediment and Transfer of Material in the Estuary. Academic Press, New York, pp 347–364

Hsu MH, Kuo AY, Kuo JT, Liu, WC (1996, 1997) Study of tidal characteristics estuarine circulation and salinity distribution in Tanshui River system (I), (II). Technical Report No. 239 and 273, Hydrotech Research Institute, National Taiwan University, Taipei, Taiwan (in Chinese)

Hsu MH, Kuo AY, Kuo JT, Liu WC (1999) Procedure to calibrate and verify numerical models of estuarine hydrodynamics. J Hydraul Eng ASCE 125:166–182

Krone RB (1978) Aggregation of suspended particles in estuaries. In: Kjerfve P (ed) Estuarine Transport Processes. University of South Carolina Press, Columbia, South Carolina, pp 177–190

Kuo AY, Nichols M, Lewis J (1978) Modeling sediment movement in the turbidity maximum of an estuary. Bulletin 111, Virginia Water Resources Research Center, Virginia Polytechnic Institute and State University, Blacksburg, VA

Liu WC, Hsu MH, Kuo AY, Kuo JT (2001) The influence of discharge on salinity intrusion in the Tanshui estuary. J Coastal Res 17:544–552

Mellor GL, Yamada T (1982) Development of a turbulence closure model for geophysical fluid problems. Rev Geophy 20:851–875

Olphen H van (1963) An introduction to clay colloid chemistry. Interscience Publishers, New York

Partheniades E (1965) Erosion and deposition of cohesive soils. J Hydraul Div ASCE 91:105–139

Postma H (1967) Sediment transport and sedimentation in the estuarine environment. Am Assoc Adv Sci 83:158–179

Water Resources Planning Commission (1999) Hydrological year book of Taiwan (in Chinese)

Wollast R (1986) The Scheldt estuary, pollution of the North Sea–An assessment. Salomon W, Bayne BL, Duursma EK, Forstner U (eds) Springer–Verlag, Berlin Heidelberg New York, pp 183–193